Proceedings of the ASME 2013 11th Fuel Cell Science, Engineering and Technology Conference
FuelCell2013
July 14-19, 2013, Minneapolis, MN, USA

FuelCell2013-18209

EFFECT OF MEMBRANE PROPERTIES ON DYNAMIC BEHAVIOR OF POLYMER ELECTROLYTE MEMBRANE FUEL CELLS

Atul Verma and Ranga Pitchumani*
Advanced Materials and Technologies Laboratory
Department of Mechanical Engineering
Virginia Tech
Blacksburg, Virginia 24061-0238

ABSTRACT

Understanding the performance of proton exchange membrane (PEM) fuel cells is critical to the water management in the fuel cell system. Low-humidity operating conditions present a complex interaction between dynamic behavior and water transport owing to different time scales of water transport mechanisms in the transient process. Toward understanding the effects of membrane properties on the dynamic behavior, this paper presents numerical simulations for a single channel PEM fuel cell undergoing changes in load, by subjecting the unit cell to step change in current. The objective is to elucidate the complex interaction between cell voltage response and water transport dynamics for various membrane properties, where the performance is critically related water content of the membrane. Detailed computational fluid dynamics (CFD) simulations are carried out to show that step increase in current density leads to anode dryout due to electro-osmotic drag, and investigate its dependence on variations in membrane properties.

INTRODUCTION

The need for energy efficient, clean and quiet, energy conversion devices for mobile and stationary applications has presented proton exchange membrane (PEM) fuel cells as a potential energy source for mobile and stationary applications. Due to major improvements in catalyst loading and membrane technology, PEM fuel cells have seen increased usage in various applications. A further reduction in cost can be achieved through better design, improved performance and durability of the fuel cells. This objective has generated lot of interest for research in control and optimization of transport and electrochemical processes of fuel cells [1,2]. While most of the research has been focused on steady-state operation, use of PEM fuel cells for automotive applications, where there are rapid changes in load, presents a need for better understanding of transient behavior.

A PEM fuel cell is composed of membrane electrode assembly (MEA), sandwiched between porous gas diffusion layers (GDL) on either side, and bipolar plates with grooved-in gas channels of serpentine or interdigitated configurations. Humidified hydrogen (H_2) and oxygen (O_2) or air are transported, through anode and cathode flow channels, respectively, and are flowed through diffusion layers to react at the catalyst layers of the MEA. Hydrogen dissociates at the anode catalyst to produce protons that are transported across the thickness of the membrane to the cathode catalyst later where it combines with oxygen and electrons, flowing through an external circuit from the anode catalyst layer to the cathode catalyst layer, to produce water.

The performance of a fuel cell is critically related to the membrane hydration, as it affects the proton conductivity through membrane—a higher water content (number of water molecules per sulfonic acid group) in the membrane ensures higher conductivity. Under low-humidity operation, suitable for automotive applications, electro-osmotic drag, back-water diffusion and rate of water supply or removal through humidified reactants, each associated with different time scales, interact in complex ways to affect the transient behavior of PEM fuel cells. The step increase in current density causes the anode side of the membrane to quickly dryout owing to electro-osmotic drag whereas back-diffusion of water from cathode to anode takes longer to rehydrate the membrane. This can lead to temporary dryout and hence sharp voltage drop, owing to jump in membrane resistance. As the back-diffusion rehydrates the anode side, the voltage recovers, improving the performance. The above transient behavior is strongly dependent on the transport and physical properties of the membrane namely, the water diffusion coefficient, electro-osmotic drag coefficient, thickness and equivalent weight, and needs to be studied in detail. Understanding the transient behavior and effect of membrane properties is of paramount importance for PEM fuel cells to be successfully deployed for mobile applications [1,9].

Several researchers have attempted to study the transient behavior of PEM fuel cells numerically. Previous numerical studies used simplified models and lacked detail represen-

* Corresponding author. +1 540 231 1776; pitchu@vt.edu

tation of complex interactions during transient operations. The model by Um et al. [3] assumed constant water content and investigated the transient response of fuel cell, emphasizing the effects of reactant diffusion. Amphlett et al. [4] developed a lumped-parameter based thermal model to predict the transient response, while using steady-state electrochemical kinetics. Pathapati et al. [5] and Xie et al. [6] developed simplified system level models for their transient study. Ceraolo [7] used a simplified one dimensional model to study the dynamic behavior, considering only the cathode side. A more complete model was developed by Wang and Wang [8,9], extending the model used in Ref. [3] to include the effects of water accumulation and electrochemical double layer discharge. The transient model explored the dynamic behavior for step change in humidity, voltage and current, emphasizing the different time scales characteristic to transport and electrochemical process. To the authors' knowledge, Wang and Wang [9] were the first to simulate the effects of step changes in current load.

In the present study, computational fluid dynamics (CFD) simulations are carried out using the model developed in Ref. [9] to study the effect of step change in current density. Although the work by Wang and Wang [9] provides mathematically rigorous description of the governing physics, the transport properties vary extensively with orders of magnitude in difference and have not been addressed in detail in previous numerical studies. Majsztrik [10] presented an elaborate compilation of the values of diffusivity of water in Nafion and the experimental techniques used, with values spanning over three orders of magnitude, at single temperature. The variations in water uptake, electro-osmotic drag coefficient, ionic-conductivity of membrane have been presented in Refs. [11], [12] and [13], respectively. The variations in the physical and transport properties of GDL and membrane play an important role in determining the transient behavior of membrane and are addressed in detail in the present study.

MATHEMATICAL MODEL

Figure 1(a) shows a schematic view of the two-dimensional section of a single channel PEM fuel cell corresponding to the geometry of the model considered in this study. Bipolar plates, gas channels, gas diffusion layers and catalyst layers on anode and cathode sides of a membrane constitute the different regions for this study. A comprehensive two-dimensional, single phase, transient, isothermal model is assumed following the assumptions in Refs. [1,8,9] to simulate the fuel cell dynamics, with the objective of accurately capturing the transient water content distribution in the membrane. The model takes into consideration important transient processes such as gas transport, water accumulation, and electrochemical double layer discharge. The 2D model assumes the variation in flow along the width of the channel to be negligible, thus over predicting the reactant concentration and current density, on an average. 2D models have been used by several researchers [3,14] and closely match experimental values. A single-channel of the fuel cell forms the computational domain for this study. The equations governing the dynamics of fuel cell behavior are as follows [8,9,14]:

Continuity: $$\nabla.\vec{u} = 0 \qquad (1)$$

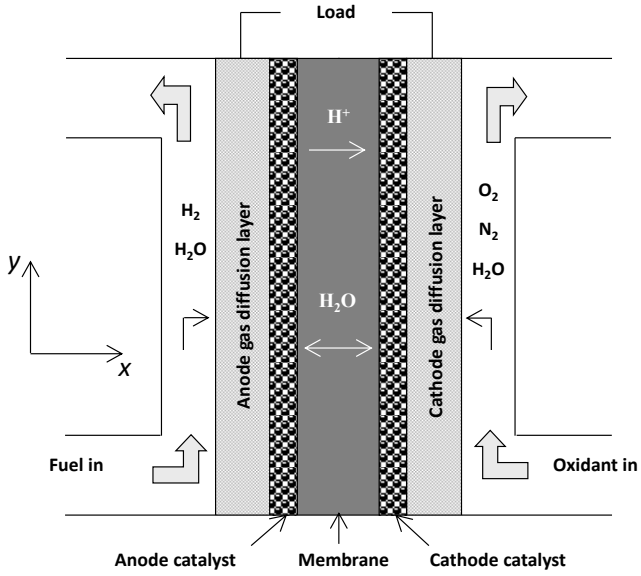

Figure 1: Schematic of polymer electrolyte membrane (PEM) fuel cell.

Momentum: $$\frac{1}{\varepsilon}\left[\frac{\partial \vec{u}}{\partial t}+\frac{1}{\varepsilon}\nabla.(\vec{u}\vec{u})\right]=-\nabla\left(\frac{p}{\rho}\right)+\nabla.\tau+S_u \qquad (2)$$

Species: $$\varepsilon\frac{\partial C_k}{\partial t}+\nabla.(\vec{u}C_k)=\nabla.(D_k^{eff}\nabla C_k)+S_k \qquad (3)$$

Charge Transport: $$\nabla.(\sigma_i^{eff}\nabla\phi_i)+S_i=0;\ i=s,m \qquad (4)$$

where $\vec{u}$ is the superficial velocity vector or volume averaged velocity, ε is the porosity of the porous media and equals unity in gas channels, p is the pressure, τ is the stress tensor, ρ represents the density, C_k denotes the molar concentration of species k namely, H_2, O_2 and H_2O, and the effective diffusivity D_k^{eff} is given by $D_k^{eff}=\varepsilon_{eff}^{1.5}D_k$ [15], where D_k is the diffusivity of each species and can be expressed as a function of temperature T and pressure p as

$$D_k = D_{k,ref}\left(\frac{T}{353}\right)^{1.5}\left(\frac{1}{p}\right) \qquad (5)$$

Eq. (3) is used to describe water transport in MEA by expressing ε as [8,9]

$$\varepsilon=\varepsilon_g+\varepsilon_m\frac{\mathrm{d}C_w^m}{\mathrm{d}C_w}=\varepsilon_g+\varepsilon_m\frac{\rho_m}{EW}\frac{RT}{p^{sat}}\frac{\mathrm{d}\lambda}{\mathrm{d}a} \qquad (6)$$

where ρ_m is the density of the dry membrane, subscripts g and m, respectively, represent gas and membrane phase, R is the universal gas constant, and EW is the equivalent weight of the dry membrane, taken to be 1.1 kg/mol. The membrane water content, λ, can be calculated from [16]:

$$\lambda=\begin{cases}0.043+17.81a-39.85a^2+36.0a^3, & 0\le a\le 1\\ 14+1.4(a-1), & 1\le a\le 3\\ 16.8, & 3<a\end{cases} \qquad (7)$$

in which, the water activity a is given by:

$$a=\frac{C_w RT}{p^{sat}} \qquad (8)$$

where the saturation pressure of water is obtained from Ref. [8] as

$$\log_{10} p^{sat} = -2.1794 + 0.02953(T - 273.15) - \quad (9)$$
$$9.1837\times10^{-5}(T-273.15)^2 + 1.4454\times10^{-7}(T-273.15)^3$$

The diffusivity of water in membrane is given by [17]:

$$D_w^m = \begin{cases} 3.1\times10^{-7}\lambda(e^{0.28\lambda}-1)e^{-2346/T} & 0 \le \lambda \le 3 \\ 4.17\times10^{-8}\lambda(1+161e^{-\lambda})e^{-2346/T} & \lambda > 3 \end{cases} \quad (10)$$

A constant density is assumed with no mass source terms, following the assumptions in Refs. [8,9]; The source term, S_u in Eq. (2), incorporates the effect of porous media on flow and is expressed in Table 1; The subscripts s and m in Eq. (4) represent the solid and membrane phases, respectively, ϕ_i is the i-phase potential, σ_i^{eff} represents effective charge conductivity for the i-th phase, and the source term S_i is a function of the transfer current density (j) in the catalyst layers and is expressed in Table 1. The ionic conductivity of the membrane σ_m is given by [16]:

$$\sigma_m = (0.005139\lambda - 0.00326)\exp\left[1268\left(\frac{1}{303}-\frac{1}{T}\right)\right] \quad (11)$$

The current generation in the catalyst layers is governed by the Butler-Volmer equation, which can be expressed in a simplified form as

$$j_a = j_a^{ref}\left(\frac{C_{H_2}}{C_{H_2}^{ref}}\right)^{1/2}\left(\frac{\alpha_a+\alpha_c}{RT}.F.\eta\right) \text{ and,}$$

$$j_c = -j_c^{ref}\left(\frac{C_{O_2}}{C_{O_2}^{ref}}\right)\exp\left(\frac{\alpha_c F\eta}{RT}\right)$$

where subscripts a and c denote anode and cathode, respectively, j^{ref} is the reference volumetric exchange current density, α is the transfer coefficient, and C_{O_2} are the molar concentrations of H_2 and O_2, respectively, F is the Faraday constant, and η is the surface over-potential given by $\eta = \phi_s - \phi_m - V_{ref}$ where V_{ref} is 0 at the anode and is equal to the open circuit voltage, V_{OCV}, at the cathode, given in terms of temperature T as $V_{ocv} = 1.23 - 0.9\times10^{-3}(T-298)$.

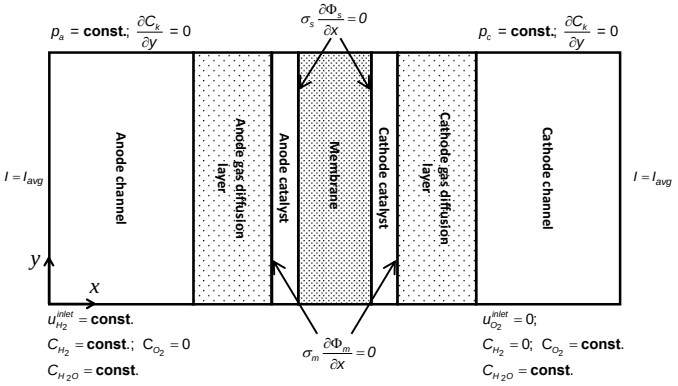

Figure 2: Schematic of model domain and associated boundary conditions.

Equations (1) to (4) form a complete set of governing equations with nine unknowns: $\vec{u}$ (three components), p, C_{H_2}, C_{O_2}, C_{H_2O}, ϕ_s, ϕ_m. The governing equations are subject to appropriate boundary and interface conditions, shown in Fig. 2. At the flow inlet boundaries, $u_{H_2}^{inlet} = 0.1947\ \text{m/s}$, $u_{Air}^{inlet} = 0.3574\ \text{m/s}$, $RH_a^{inlet} = 100\%$, and $RH_c^{inlet} = 0\%$. Owing to low Reynolds number of the flow in gas channels, approximately 500, laminar flow is used for simulations.

Table 1: Source terms in the governing equations

Domain	S_v	S_i	S_s, S_m
Gas channels	0	0	0
Diffusion layers	$-\frac{\mu}{K_{GDL}}\vec{u}$	0	0
Catalyst layers	$-\frac{\mu}{K_{CL}}\vec{u}$	anode: $-\frac{j_a}{2F}$ $(i = H_2)$ 0 $(i = O_2)$ $-\nabla.\left(\frac{n_d\, i_e}{F}\right)$ $(i = H_2O)$ cathode: 0 $(i = H_2)$ $-\frac{j_c}{4F}$ $(i = O_2)$ $\frac{j_c}{2F} - \nabla.\left(\frac{n_d\, i_e}{F}\right)$ $(i = H_2O)$	anode: $S_s = -j_a < 0$ $S_m = +j_a > 0$ cathode: $S_s = +j_c > 0$ $S_m = -j_c < 0$
Membrane	$-\frac{\mu}{K_{CL}}\vec{u}$	0	0

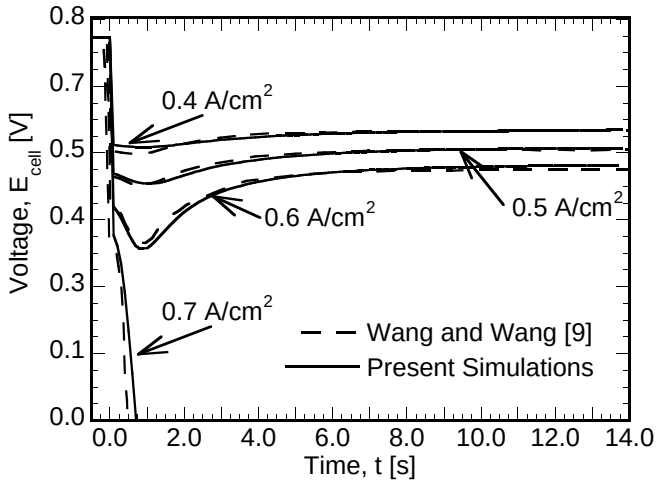

Figure 3: Validation of numerical model of PEM with data from Ref. [9].

Table 2. Geometrical and physical parameters used in the numerical simulations [8,9,14]

Parameter [units]	Symbol	Value
Gas channel depth [mm]		1.0
Diffusion layer thickness [mm]		0.3
Catalyst layer thickness [mm]		0.01
Membrane (N112) thickness [mm]		0.051
Fuel cell/ Gas channel length [mm]		100.0
Temperature [K]	T	353
Permeability of diffusion layer [m^2]	K_{GDL}	10^{-12}
Permeability of catalyst layer [m^2]	K_{CL}	10^{-15}
Gas diffusion layer porosity	ε_{GDL}	0.6
Catalyst layer porosity	ε_{CL}	0.4
Volume fraction membrane in catalyst layer	ε_m	0.26
Anode reference exchange current density [A/m^3]	$j_{a,\,ref}$	5.00 x 10^8
Cathode reference exchange current density [A/m^3]	$j_{c,\,ref}$	500
H_2 diffusivity membrane [m^2/s]	$D_{H_2,\,mem}$	2.59 x 10^{-10}
H_2 diffusivity in gas [m^2/s]	$D_{H_2,\,ref}$	1.1 x 10^{-4}
O_2 diffusivity in membrane [m^2/s]	$D_{O_2,\,mem}$	1.22 x 10^{-10}
O_2 diffusivity in gas [m^2/s]	$D_{O_2,\,ref}$	3.2348 x 10^{-5}
H_2O diffusivity in gas [m^2/s]	$D_{H_2O,\,ref}$	7.35 x 10^{-5}
O_2 diffusivity in membrane [m^2/s]	$D_{O_2,\,mem}$	8.328 x 10^{-10}

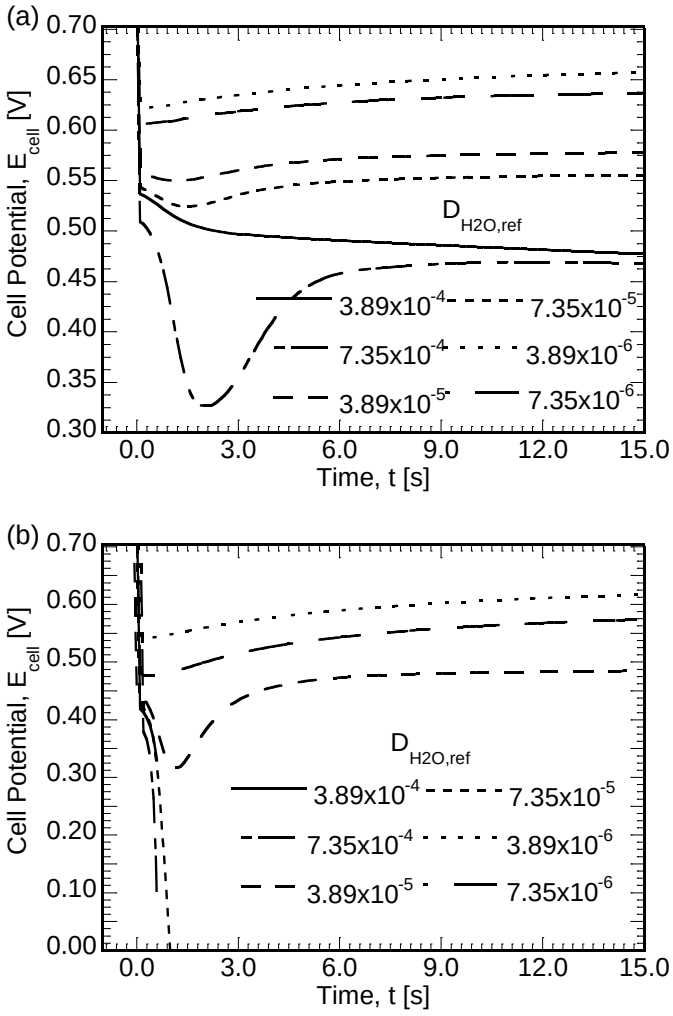

Figure 4: Variation in cell voltage as a function of time, for various H_2O diffusivity values, for step change in current from (a) 0.1 to 0.4 A/cm^2 and (b) 0.1 to 0.6 A/cm^2.

The governing equations (1) to (4), with above the boundary conditions are solved using a control volume based commercial fluid dynamics (CFD) package, Fluent® using the pressure-implicit with splitting of operators (PISO) algorithm, a pressure-based segregated algorithm [18] . The specific governing equations and the corresponding source terms are implemented through user-defined functionsand user-defined scalars (species and phase potentials). A systematic mesh size convergence check was conducted such that the difference in the results was less than 0.5% for further reduction in mesh size. About 3,500 computational cells are used to capture the detailed electrochemical and physical phenomenon. In order to accurately capture the anode dryout and voltage reversal, a maximum time step of 0.1 s was found to be optimal for the simulations. A constant time step of 0.1 s is used for the simulations; with a run time of approximately 6 hours on an Intel® Xeon™ Processor 3.33 GHz. A load change is imposed at the initial time, t = 0, by specifying the change in the current density, I , as a boundary condition. The geometrical, physical and electrochemical parameters used in this study are listed in Table 2.

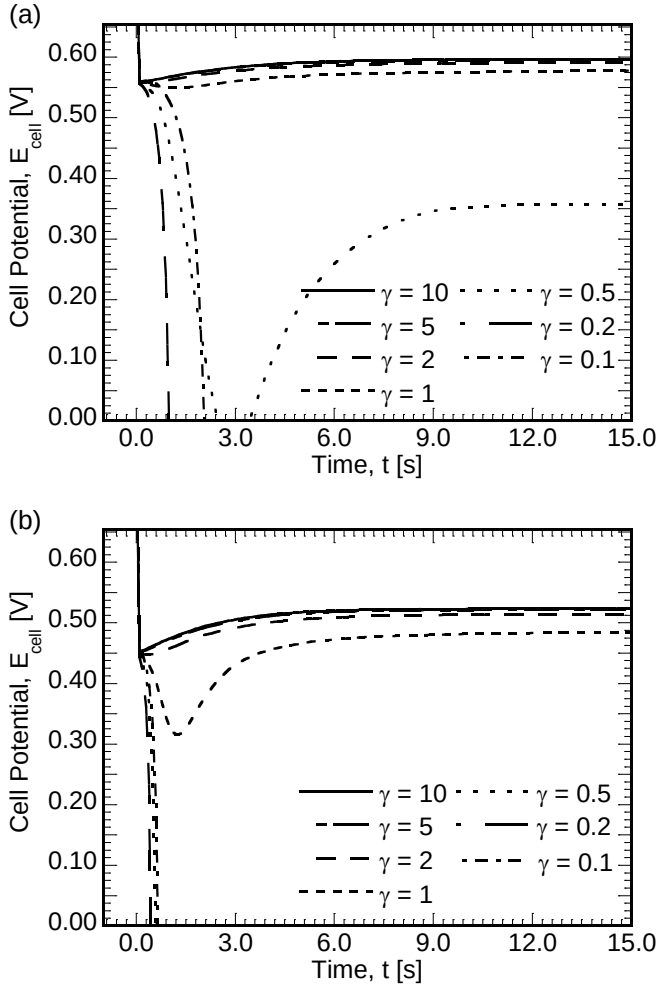

Figure 5: Variation in cell voltage as a function of time, for various water diffusivity values in membrane, for step change in current from (a) 0.1 to 0.4 A/cm^2 and (b) 0.1 to 0.6 A/cm^2

RESULTS AND DISCUSSION

The numerical model described in the previous section is first validated by comparing the cell voltage (E_{cell}) response with the numerical results reported by Wang and Wang [9].

Figure 3 shows the cell voltage response for step change in current density from I = 0.1 to 0.4, 0.5, 0.6, 0.7 A/cm^2, where the solid lines represent the results from present simulations, and the results from Ref. [9] are indicated by dashed lines. It can be seen that the cell voltage drops instantaneously owing to the time-scale associated with the electrochemical double layer discharge, on the order of micro-to-milli-seconds. In addition, at low-humidity operating conditions, the voltage response exhibits an undershoot, with the degree of undershoot increasing as the magnitude of current change is increased, and can be seen in Fig. 3. For I = 0.7 A/cm^2, Fig. 3 shows that the voltage drops to zero, indicating a voltage reversal. The above behavior of undershoot can be attributed to the jump in water electro-osmotic drag, which increases proportionally to the jump in the current density. This causes the anode-side to dryout, increasing membrane resistance leading to further drop in voltage reaching a minimum. As the membrane at anode is rehydrated, the membrane resistance decreases, leading to increase in voltage and achieving steady state upon hydration of membrane. The time scale associated with the back-diffusion of water dictates the time taken for the voltage response to improve, and is of the order of 0.7 s for the current case. The figure shows close agreement between the voltage response obtained for present simulations and those reported in Ref. [9]. The comparisons presented, therefore, demonstrate the capabilities of the present model to accurately capture the water transport dynamics and predict voltage response.

The effects of membrane properties, namely water diffusivity, electro-osmotic drag coefficient, equivalent weight and water diffusivity in the porous media or gas, on voltage response, for step change in current density, is studied and presented in detail in this section.

Figures 4 (a) and (b) present the temporal variation in cell potential for various H_2O diffusivity values in gas as the current density is stepped up from 0.1 A/cm^2 to 0.4 A/cm^2 and from 0.1 A/cm^2 to 0.6 A/cm^2, respectively. From Fig. 4(a) it is observed that, following the instantaneous drop in cell voltage which is attributed to the time scale associated with electrochemical double layer discharge as explained before, the cell voltage recovers after an undershoot reaching a steady state, for all the diffusivity values except for $D_{H_2O,ref} = 7.35\times10^{-6}$. For $D_{H_2O,ref} = 7.35\times10^{-6}$, the degree of voltage undershoot is maximum, with voltage reaching a minimum at t = 2 s, as seen in Fig. 4a. In contrast to that observed in Fig. 4(a), for a step change in current density from 0.1 A/cm^2 to 0.6 A/cm^2 (Fig. 4(b)) voltage reversal occurs for the diffusivity values of $D_{H_2O,ref} = 3.89\times10^{-4}$, 7.35×10^{-5} and 7.35×10^{-6} resulting from anode dryout, while significant voltage undershoot is observed for $D_{H_2O,ref} = 3.89\times10^{-5}$ which is recovered with back-diffusion. It is noted here that although the properties of membrane are fixed change in diffusivity values of water in porous layers presents a complex dynamic behavior affecting the time scales for voltage recovery. It can be seen in Fig. 4(a) and 4(b), that there exists a non-monotonic trend associated with variation in steady state cell potential values for different diffusivity values, with $D_{H_2O,ref} = 3.89\times10^{-6}$ and 7.35×10^{-6} defining the maximum and minimum values of steady state voltages in Fig. 4(a). Therefore, it can be established that water diffusion through porous layers significantly affects the water distribution process, thus determining the voltage response for change in current.

Following the same format in Fig. 4, Figs. 5(a) and (b) depict the change in cell potential over time for different values of membrane diffusivity as the current density is changed as a step from 0.1 A/cm^2 to 0.4 A/cm^2 and from 0.1 A/cm^2 to 0.6 A/cm^2, respectively. The water diffusivity in membrane D_m^w is a function of the membrane water content, λ and temperature, T as defined in Eq. (10). The effect of variation in membrane diffusivity is studied by varying γ in Fig. 5, which represents the factor by which the diffusivity is increased over the base value. For instance, $\gamma = 2$ refers to diffusivity values of $2\times D_m^w$ and $\gamma = 1$, pertains to the definition in

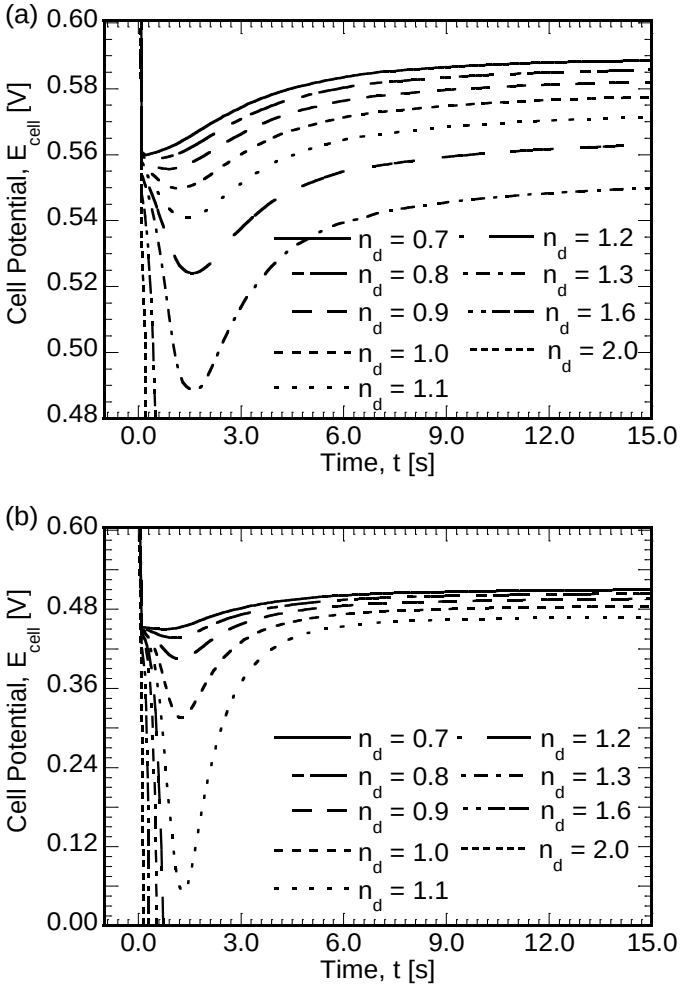

Figure 6: Variation in cell voltage as a function of time, for various values of electro-osmotic drag coefficient, for step change in current from (a) 0.1 to 0.4 A/cm^2 and (b) 0.1 to 0.6 A/cm^2.

Eq. (10). In the present study γ is varied from 0.1 to 10 for the two cases described above. The above values are chosen to provide a systematic study, whereas using the data reported in the literature discussed before would be cumbersome and hence is avoided. As seen from Figs. 5(a) and 5(b), the voltage reversal occurs for γ < 1.0, while in Fig. 5(a) it can be seen that $\gamma = 0.5$ almost defines the limiting case for voltage reversal. This is attributed to a higher magnitude of step change in current density from 0.1 to 0.6 A/cm^2 in Fig. 5(b), leading to a voltage reversal at relatively high diffusivity value compared to Fig. 5(a). Also, it is noted that for $\gamma = 1.0$ the degree of undershoot observed is much higher in Fig. 5(b) compared to that observed in Fig. 5(b). Although, voltage reversal also occurs for $\gamma = 0.5$, for a step change in current density from 0.1 A/cm^2 to 0.4 A/cm^2 (Fig. 5 (a)), the cell voltage recovers upon rehydration, after a reversal period from t = 2.5 to 3.5 s. For higher diffusivity values no undershoot is observed and the cell reaches steady state following the expected initial instantaneous decrease in cell voltage, as illustrated in Figs. 5 (a) and (b) for γ values of 2 and higher. This behavior can be attributed to the increased transport rate of water generated at cathode to anode through back-diffusion.

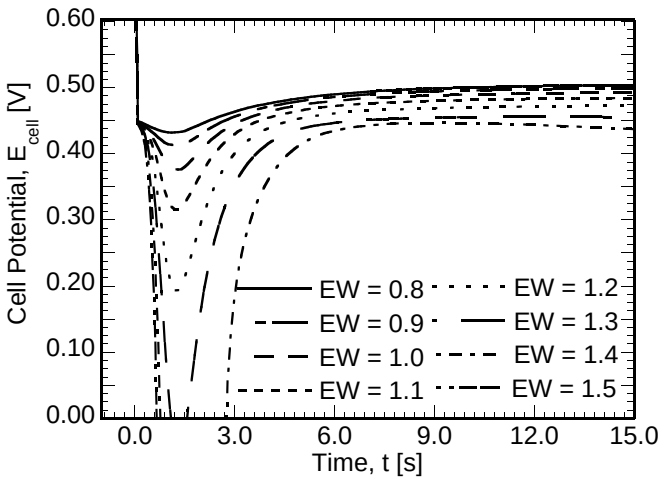

Figure 7: Variation in cell voltage as a function of time, for various equivalent weight (*EW*) values, for step change in current from 0.1 to 0.6 A/cm^2.

Figures 6(a) and (b) show the temporal variation in cell potential for various electro-osmotic drag coefficient, n_d, values as the current density undergoes a step change from 0.1 A/cm^2 to 0.4 A/cm^2 and from 0.1 A/cm^2 to 0.6 A/cm^2, respectively. The electro-osmotic drag coefficient gives a representative figure of the effective moles of water transported per mole of protons conducted from anode to cathode catalyst layer and appears as a source term (Table 1) in species conservation equation for water Eq. (4). The values of n_d used in the present study range from 0.7 to 2.0, in accordance with the values reported in literature. Higher values of n_d indicate more water being transported from anode to cathode for a specified current. It can be seen in Fig. 6(a) that cell voltage reaches zero for n_d >1.3 whereas owing to increase in current density to 0.6 A/cm^2 in Fig. 6(b), the voltage reaches zero and finally reverse for n_d >1.1. The steady state cell voltage values for both 0.4 A/cm^2 [Fig. 6(a)] and 0.6 A/cm^2 [Fig. 6(b)] exhibit monotonic trend for variation in n_d. Also, it can be seen that degree of voltage undershoot is relatively smaller in Fig. 6(a) compared to that observed in Fig. 6(b).

Figure 7 shows the cell voltage response for change in current density from 0.1 to 0.6 A/cm^2, for various equivalent weights, *EW*. The results presented earlier were based on *EW* = 1.1 and Fig. 7 shows the effect of varying *EW* from 0.8 to 1.5. The *EW* represents equivalent molecular weight of dry membrane in kg/mol, with lower values of *EW* indicating higher moles per kg, and, in turn, increased number of sulfonic acid groups. Increase in number of sulfonic acid groups leads to an increase in the amount of water stored in the unit mass membrane, for a given water activity. An increase in *EW* leads to a decrease in the amount of water that can be accumulated by membrane for a given water activity. It can be seen in Fig. 7 that with increase in *EW* from 0.8 to 1.1 the degree of undershoot increases with voltage reversal for *EW* > 1.1. The above behavior can be attributed to a faster dryout of anode side of the membrane, with increase in *EW*, as the same amount of water is dragged to the cathode but the holding capacity is reduced with increase in *EW*. As previously observed in Fig. 6, the steady state cell voltage values vary monotonically with

EW. It is also noted from Fig. 7 that with increase in *EW* the time taken for the membrane to rehydrate also increases. The time taken by the cell potential to reach a steady state value is dependent on the time scale associated with time constant for membrane hydration, which is inversely proportional to *EW*.

The results presented in this section offer insight into the effects of various membrane properties on the hydration of the membrane during transient operation of fuel cells. The detailed investigation indicates that for step change in current, the anode side gets dehydrated owing to electro-osmotic drag subjecting the cell to voltage reversal at instances and is strongly correlated to membrane properties. The work correlates transport properties and cell voltage response, thus providing insight in to the design of membranes for desired applications. Future work could include a study of various existing membranes, such as reinforced membranes, hydrocarbon membranes and others, using the present model. The model can also be used to study the dry startup behavior of PEM fuel cells and to optimize operating parameters to improve performance as it closely emulates the actual load changes for automotive applications.

CONCLUSIONS

A comprehensive analysis of the effects of membrane properties on the cell voltage response of a single-channel PEM fuel cell was presented, based on the numerical simulations for low humidity operations. It was shown that a sudden increase in current density can lead to anode dryout, causing voltage reversal and may lead to cell degradation. The voltage response was shown to be a strongly correlated to the membrane properties and also the water diffusion in porous media. The results provide insight in designing and choosing membranes for particular applications.

Nomenclature

A	superficial electrode area [m^2]
C_k	molar concentration of species k [mol/m^3)]
D	mass diffusivity of species [m^2/s]
E_{cell}	cell potential or voltage [V]
EW	equivalent weight of dry membrane [kg/mol]
F	Faraday Constant [96,487 C/equivalent]
j	transfer current [A/m^3]
K	permeability [m^2]
n_d	electro-osmotic drag coefficient [H_2O/H^+]
p	pressure [bar]
R	Universal gas constant [8.314 J/mol K]
RH	relative humidity
S	source term in transport equations
T	temperature [K]
$\vec{u}$	velocity vector

Greek letters

α	transfer coefficient
ε	porosity
η	surface overpotential [V]
λ	membrane water content
μ	viscosity [kg/m s]
ρ	density [kg/m^3]
σ	electronic conductivity [S/m]
τ	shear stress [N/m^2]; time constant; tortuosity
ϕ	phase potential [V]

Superscripts and subscripts

a	anode
c	cathode
cell	single fuel cell
e	electrolyte
eff	effective value
eq	equivalent
g	gas phase
inlet	inlet
k	species
m	membrane phase
o	t=0 s, initial state
ref	reference value
s	electronic phase
sat	saturated value
SS	steady state
t	time > 0 s
w	water

References

[1] Wang, C.Y., 2004, "Fundamental Models for Fuel Cell Engineering," *Chemical Reviews*, **104**, pp. 4727-4766.

[2] Perry, M.L., Fuller, T.F., 2002, "A Historical Perspective of Fuel Cell Technology in the 20th Century," *J. Electrochemical So.*, **149 (7),** pp. S59-67.

[3] Um, S., Wang, C. Y., Chen, K.S., 2000, "Computational Fluid Dynamics Modeling of Proton Exchange Membrane Fuel Cells," *J. Electrochemical So.*, **147 (12),** pp. 4485-93.

[4] Amphlett, J.C., Mann, R.F., Peppley, B.A., Roberge, P.R., Rodrigues, A., 1996, "A Model Predicting Transient Response of Proton Exchange Membrane Fuel Cells," *Journal of Power Sources*, **61(1-2),** pp. 183-188.

[5] Pathapati, P.R., Xue, X., Tang, J., 2005,**"**A New Dynamic Model for Predicting Transient Phenomena in a PEM Fuel Cell System," *Renewable Energy*, **30,** pp. 1-22

[6] Xue, X., Tang, J., Smirnova, A., England, R., Sammes, N., 2004, "System level lumped-parameter dynamic modeling of PEM Fuel Cell," *Journal of Power Sources*, **133(2),** pp. 188-204.

[7] Ceraolo, M., Miulli, C., Pozio, A., 2003, "Modelling Static and Dynamic Behaviour of Proton Exchange Membrane Fuel Cells on the Basis of Electro-Chemical Description," *Journal of Power Sources*, **113(1),** pp. 183-188.

[8] Wang, Y., Wang, C.Y., 2005, "Transient Analysis of Polymer Electrolyte Fuel Cells," *Electrochem. Acta*, **50**, pp. 1307-1315

[9] Wang, Y., Wang, C.Y., 2006, "Dynamics of Polymer Electrolyte Fuel Cells Undergoing Load Changes," *Electrochem. Acta*, **51**, pp. 3924-33

[10] Majsztrik, P.W., 2008, "Mechanical and Transport Properties of Nafion for PEM Fuel Cells; Temperature and Hydration Effects," *PhD Thesis, in: Chemistry*, Princeton

University, Princeton, NJ, pp. 103
[11] Zawodzinski, T.A., Springer, T.E., Uribe, F., Gottesfeld, S., 1993, "Characterization of Polymer Electrolytes for Fuel Cell Applications," *Solid State Ionics*, **60,** pp. 199-221.
[12] Slade. S., Campbell, S.A., Ralph, T.R., Walsh, F.C., 2002, "Ionic Conductivity of an Extruded Nafion 1100 EW Series of Membranes," *J. Electrochemical So.*, **149 (12)**, pp. A1556-64.
[13] Zawodzinski, T.A., Derouin, C., Radzinski, S., Sherman, R., Smith, V.T., Springer, T.E., Gottesfeld, S., 1993, "Water Uptake by and Transport through Nafion 117 Membranes," *J. Electrochemical So.*, **140 (12)**, pp. 1041-47.
[14] Zhang, Y., Mawardi, A., Pitchumani, R., 2006, "Effects of Operating Parameters on the Uniformity of Current Density Distribution in Proton Exchange Membrane Fuel Cells," ASME *Journal of Fuel Cell Science and Technology*, **3(4)**, pp. 464-476
[15] Bird, R.B., Stewart, W.E., Lightfoot, 1960, E.N., *Transport Phenomena*, Wiley, New York.
[16] Springer, T.E., Zawodzinski, T.A., Gottesfeld, S., 1991, "Polymer Electrolyte Fuel Cell Model," *J. Electrochemical So.*, **138 (8)**, pp. 2334-42.
[17] Motupally, S., Becker, A.J., Weidner, J.W., 2000, "Diffusion of Water in Nafion 115 Membranes," *J. Electrochemical So.*, **147 (9)**, pp. 3171-77.
[18] ANSYS® Academic Research, Release 14.0, Help System, Fluent User Guide, ANSYS, Inc.